Special Feature: Analysis Techniques to Evaluate the Next Generation Electronic Materials

Research Report

Characterization of Threading Dislocations in an Ammonothermal GaN Substrate by Synchrotron Radiation X-ray Topography and Transmission Electron Microscopy

Kayo Horibuchi, Satoshi Yamaguchi, Yasuji Kimoto, Koichi Nishikawa and Tetsu Kachi

Report received on Feb. 6, 2019

ABSTRACT Dislocation analysis was carried out on a GaN epitaxial layer on a GaN substrate fabricated using a basic ammonothermal method using synchrotron radiation X-ray topography (XRT) and transmission electron microscopy (TEM) . XRT was used to examine dislocations included in the bulk substrate and it was found that threading dislocations (TDs) were enlarged after epitaxial growth. TEM and scanning TEM (STEM) revealed that the TDs present in the GaN substrate are deformed into helical dislocations and the generation of the voids by heat treatment in the substrate for the first observation in the GaN crystal. These phenomena are formed by the interactions between the dislocations and vacancies. The helical dislocation was formed in the substrate region, and not in the epitaxial layer region. Conventional GaN crystals have a high density of dislocation; however, such crystals show no deformation. The generation of new defects was found to be driven only by heat treatment. In this study, the formation of defects similar to those found in metals, Si, and GaAs single crystals was observed, showing that the crystal quality of the GaN crystal was improved dramatically.

KEYWORDS GaN Substrate, Ammonothermal Growth, X-ray Topograph, TEM, Dislocation

1. Introduction

GaN is a promising material for use in next-generation power devices. However, to improve the electrical characteristics of GaN powered devices, it is essential to reduce the number of dislocations in GaN crystals. For this purpose, a high-quality GaN single crystal bulk substrate is required. Conventional GaN is crystalline with a high density of dislocations (of 10^6 cm^{-2} or more) due to it being epitaxially grown on foreign substrates, such as sapphire.[1,2] Recently, mass production methods that allow the synthesis of high-quality and large diameter GaN bulk crystals have been developed and various growth methods have subsequently been reported. One such preparation is the hydride vapor phase epitaxy method of vapor phase growth, in which bulk crystals are obtained by epitaxial growth on a substrate to form a thick film.[3-5] Another is liquid phase growth, such as via the Na flux[6,7] or ammonothermal methods.[8-10] These are methods for obtaining GaN crystals by the precipitation and recrystallization of GaN at high temperatures and pressures and have the potential to produce low-cost and high-quality substrates. Therefore, studies have been carried out toward the establishment and commercialization of low-cost and high-quality growth methods. To develop a GaN-based vertical power device for the automotive industry, it is necessary to clarify the crystal quality by investigating the correlation between defects and device characteristics.[11-14] For this purpose, it is important to analyze the types of crystal defects that exist and how these defects are generated. In this study, threading dislocation (TD) analysis was carried out using high-resolution monochromatic synchrotron radiation X-ray topography (XRT) and transmission electron microscopy (TEM) on a GaN epitaxial layer on a bulk GaN substrate fabricated using an ammonothermal method.

2. Experimental Procedure and Results

2. 1 XRT Measurements

Figure 1 shows the experimental procedure. The GaN substrates used were fabricated using a basic ammonothermal method, involving an O-doped n-type

substrate with a carrier concentration of 3×10^{18} cm^{-3}, a diameter of one inch, and a thickness of approximately 350 μm. The measurement conditions were as follows. First, XRT images of the GaN substrate were recorded in reflection geometry (Bragg case) at the SPring-8, BL16B2. The observed diffractions were 11−24 and 0008 using 9.02 and 10.47 keV X-rays, respectively, and the penetration depth of the X-rays was approximately 5 μm. **Figure 2**(a) shows the 11−24 diffraction topographs of the GaN substrate and these feature several large white spots and other small spots indicating the presence of two types of dislocations in the GaN substrate. In general, it has been shown that the spot size of pure-edge TDs is smaller than that of screw TDs, as observed previously in SiC.[15] Therefore, the appearance of the dislocations in GaN indicates that the crystal system is similar to that of SiC. After the XRT measurements, an epitaxial layer of approximately 5 μm in thickness was grown on the same substrate by metal-organic chemical vapor deposition (MOCVD) or just via annealing in the MOCVD reactor without any growth. Trimethylgallium (TMG), NH_3, and the carrier gases N_2 and H_2 were used as materials for the epitaxial growth at a temperature of 1100°C under atmospheric pressure and the annealing was carried out under the same conditions as the growth in the absence of TMG. After this procedure, the XRT measurements were repeated.

Figure. 2(b) shows the 11−24 diffraction topograph of the GaN wafer with the epitaxial layer in the same position as that in Fig. 2(a). Although the penetration depth of the X-rays was close to the thickness of the epitaxial layer, substrate information could also be obtained, as shown in the figure. The white spots are enlarged in Fig. 2(b) and the initial spot sizes were found to be 10–20 μm in diameter, changing to 30–50 μm after the epitaxial growth. **Figure 3**(a) is a reference that can be compared alongside Fig. 3(b), which shows the 11−24 diffraction topograph of the GaN wafer after annealing in the MOCVD reactor without any growth at the same position as Fig. 3(a). As in Fig. 2(b), the white spots in Fig. 3(b) were observed to be enlarged. Since the spot size reflects the area of the strain field around a dislocation, the change in the spot sizes indicates a significant change in the dislocation features induced by heating at a high temperature. Small spots hidden in the dark contrast in Figs. 2(b) and 3(b) can also be observed. Since the penetration

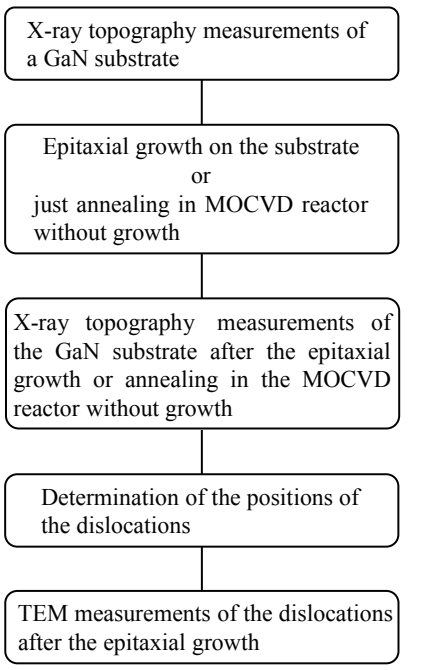

Fig. 1 Flow chart of the experimental procedure.

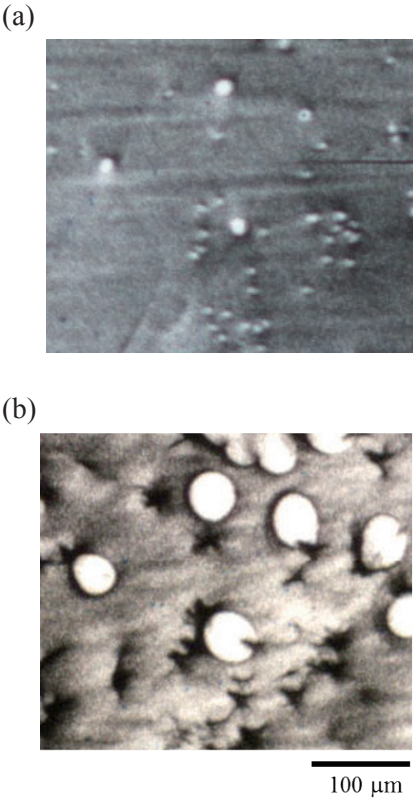

Fig. 2 11−24 diffraction topographs at the same position on the GaN wafer (a) before epitaxial growth and (b) after epitaxial growth.

depth of the X-rays is approximately 5 μm, information on the vicinity of the epitaxial layer/substrate interface can be obtained from the epitaxial layer. Therefore, there are two possible causes for the enlargement of the dislocation image in the XRT images. One is the expansion of the strain field due to deformation of the dislocation, and the other is the increase in the Burgers vector magnitude $|\boldsymbol{b}|$ of the TDs. In SiC, which is in the same crystal system as that of GaN, large defect images are frequently observed.[16] The reason behind this is the presence of TDs with large Burgers vectors ($\boldsymbol{b} = n\boldsymbol{c}$, n = 2, 3...) that are referred to as "micropipes". When a large electric field is applied to this type of dislocation, the withstanding voltage of the elements is found to deteriorate significantly.[17] However, there have been only a few reports on micropipes or nanopipes in GaN crystals;[18,19] therefore, more careful analysis is required. With this in mind, detailed TEM measurements were carried out.

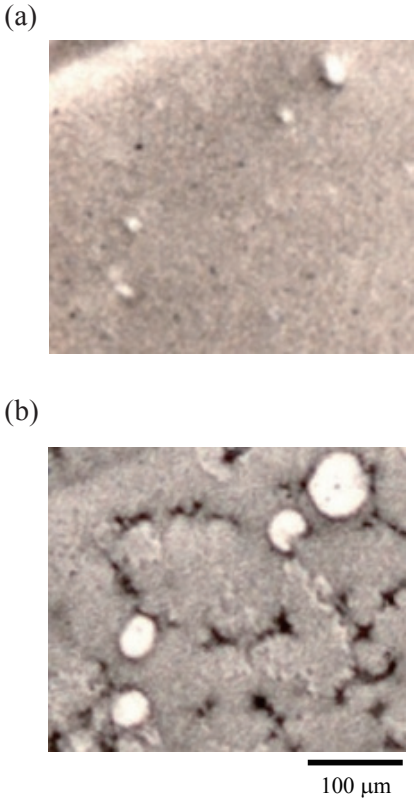

Fig. 3 11−24 diffraction topographs at the same position on the GaN wafer (a) before annealing and (b) after annealing in the MOCVD reactor without growth.

2. 2 TEM

To investigate the details of the dislocation behavior, TEM measurements were conducted. First, to observe the white spots present in the XRT images using TEM, wet etching (H_2SO_4: H_2PO_4 = 1:3, 250°C) was performed and pits were formed on the TDs. The positions of the TDs and the etched pits were matched by comparing the X-ray topographic image and the laser microscopy image of the same region, shown in **Fig. 4**. Based on the topography, the dislocation densities corresponding to the large white spots and small spots were deduced to be approximately 5×10^3 cm^{-2} and 1×10^5 cm^{-2}, respectively. Next, to process the dislocations, a cross-sectional TEM sample was prepared using a focused ion beam. TEM and scanning TEM (STEM) observations were performed using a Hitachi H-9000 NAR microscope operating at 300 kV, a JEOL JEM-2100 F(Cs) microscope operating at 200 kV, and a JEM-1000 RS microscope operating at 1000 kV. The Burgers vectors of the TDs were analyzed using the $\boldsymbol{g}\cdot\boldsymbol{b}$ method and the large-angle focused electron beam diffraction (LACBED) method. Here, the structures of the TDs present in the GaN crystal are briefly described, and the names of the TD types mentioned in this study are confirmed. Three types of TDs with the Burgers vectors $\boldsymbol{b}$ of $\boldsymbol{a}$ = <11–20>/3,

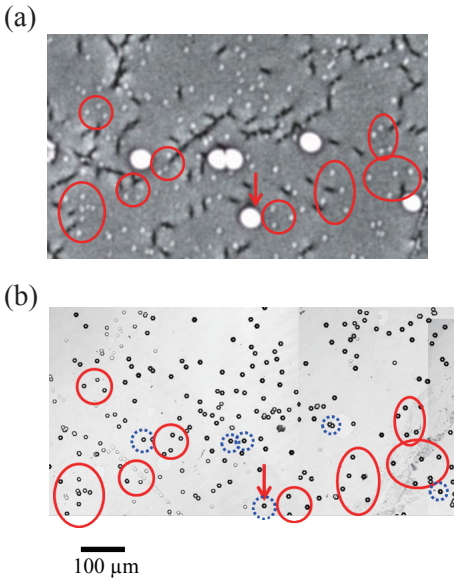

Fig. 4 (a) 0008 diffraction topograph of the GaN epitaxial layer. (b) The etched pit image of the same area shown in (a) imaged by a laser microscope.

$\boldsymbol{c}$ = <0001> and $\boldsymbol{a} + \boldsymbol{c}$ = <11−23>/3 exist in hexagonal crystals such as GaN. When TDs run parallel to a $\boldsymbol{c}$-axis, they can be referred to as edge, screw, and mixed dislocations.[20] In general, the analysis of the Burgers vector $\boldsymbol{b}$ of the dislocations was carried out using the $\boldsymbol{g}\cdot\boldsymbol{b}$ method to determine the existence/nonexistence of dislocation contrast within the TEM image by changing the diffraction vector $\boldsymbol{g}$. The identification of the dislocation type was carried out by looking at the two-beam bright-field contrast images. **Figure 5** shows cross-sectional TEM and STEM images of the etched pits before and after the etching process. The TDs before the epitaxial growth propagate straight to the surface. After the epitaxial growth, these went straight into the epitaxial layer, but were found to curve complicatedly in the substrate. **Figure 6** shows a two-beam bright field image after the epitaxial growth, where Figs. 6(a) and (b) show the large spot dislocations and **Figs. 7**(a) and (b) show the small spot dislocations in the XRT images, with these TDs being identified using the $\boldsymbol{g}\cdot\boldsymbol{b}$ method. In the case of the TDs in the epitaxial layer, the large spots TDs were identified as mixed dislocations because the contrast is present in both Figs. 6 (a) and (b) ($\boldsymbol{g}\cdot\boldsymbol{b} \neq 0$). The small spot TDs were identified as edge dislocations because the contrast is present in Fig. 7(a) and absent in Fig. 7(b). These results are consistent with the relationship between the spot diameters in the XRT images. The curved dislocations were then investigated. **Figure 8** shows the bright field scanning transmission electrons microscope (BF-STEM) image of the mixed dislocations (Fig. 5 (b)) after epitaxial growth, where Fig. 8(a) is incident on an axis and Fig. 8(b) is observed for [11−20] inclined at about 20° with respect to a rotation axis. By tilting the dislocation, it became clear that the dislocation was helical shaped. Further examination revealed that the

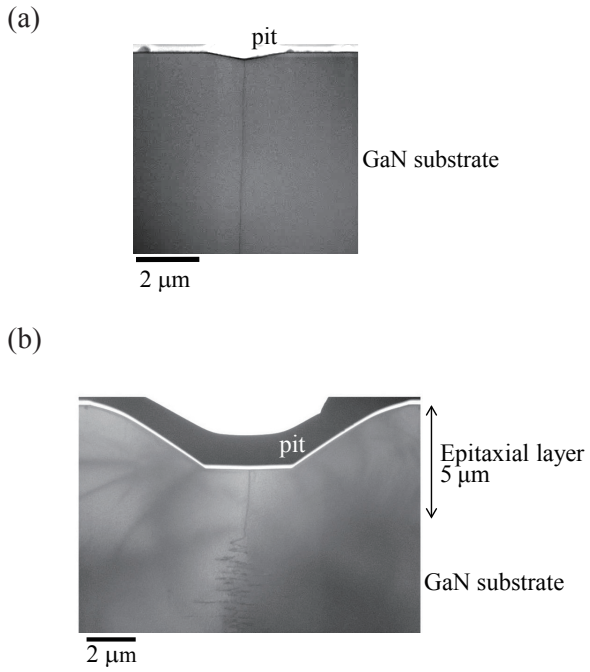

Fig. 5 Cross-sectional STEM and TEM images taken from the etched pit region (a) STEM image of the sample before epitaxial growth and (b) TEM image of the sample after epitaxial growth.

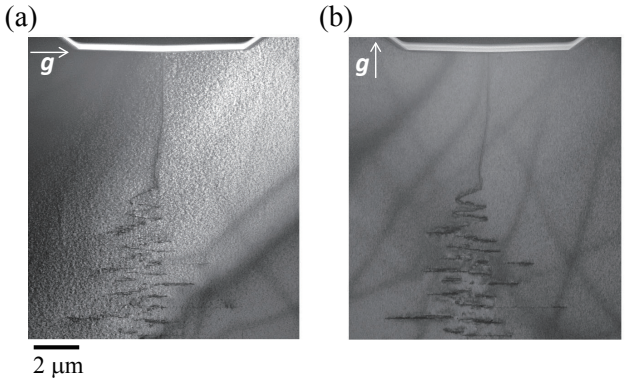

Fig. 6 Two-beam BF-TEM images taken from the area of the large spot in the XRT image after epitaxial growth with (a) $\boldsymbol{g}$ = 11−20 and (b) $\boldsymbol{g}$ = 0002 for the region shown in Fig. 5 (b).

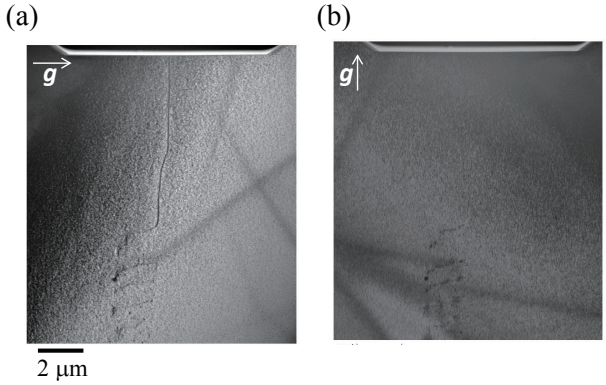

Fig. 7 Two-beam BF-TEM images taken from the area of the small spot in the XRT image after epitaxial growth with (a) $\boldsymbol{g}$ = 11−20 and (b) $\boldsymbol{g}$ = 0002.

dislocation lines were deformed stepwise and voids were observed at the steps.

Thus, the $\boldsymbol{g}\cdot\boldsymbol{b}$ method can be used to distinguish the screw and edge components, but cannot estimate the magnitude of the Burgers vector. The Burgers vector of dislocations $\boldsymbol{b}$ = [u v w] is most reliably calculated using the LACBED method,[21,22] and can be explained as follows. When the incident electron beam is intentionally defocused to irradiate the entire region containing the dislocation, the higher-order Laue zone line shows "splitting" because the Bragg condition changes due to the effect of the local strain of the dislocation. A relationship $\boldsymbol{g}\cdot\boldsymbol{b}$ = n is established between the number of splittings, n, the Burgers vector $\boldsymbol{b}$ (= [u v w]), and the diffraction vector $\boldsymbol{g}$ (= [h k l]). By counting the number of splittings from at least three reflection lines, the Burgers vector $\boldsymbol{b}$ can be determined by solving simultaneous equations. **Figure 9** shows the LACBED images. The mixed dislocations in the epitaxial layer (in Figs. 6(a) and (b)) were analyzed. **Table 1** shows the simultaneous equations obtained from $\boldsymbol{g}$ and n. Solving the simultaneous equations in Table 1 yields $\boldsymbol{b}$ = [0−11], which can be converted to the Miller–Bravais indices $\boldsymbol{b}$ = 1/3[−12−1−3]. A TD with a Burgers vector 1/3[−12−1−3] corresponds to a mixed dislocation present in a conventional GaN crystal. From these results, when the TD is transferred from the GaN substrate to the epitaxial layer, no change in the Burgers vector occurs, and the cause of the large defect image in the XRT image can be identified as being a result of the expansion of the strain field caused by the curvature of the dislocation in the GaN substrate.

3. Discussion

The reasons behind the TD deformations were identified. The mixed dislocation in Fig. 8 was found to be similar to the dislocations known as "helical dislocations" formed by the interaction of dislocations and point defects.[23] The deformation mechanism of helical dislocations has already been elucidated in metallic crystals and this phenomenon occurs when a single crystal with a low density of dislocations of high impurity content is heat-treated.[24-26] For the first time in a GaN crystal, the TD in a GaN substrate has been observed to deform into a helical dislocation by heating it to 1000°C. From the observation of the helical dislocation, it can be inferred that although the high-quality GaN crystals produced by the ammonothermal method have a low density of dislocations, they have a high density of point defects and its crystallinity is apparently different from that of GaN thin films produced by a vapor phase growth

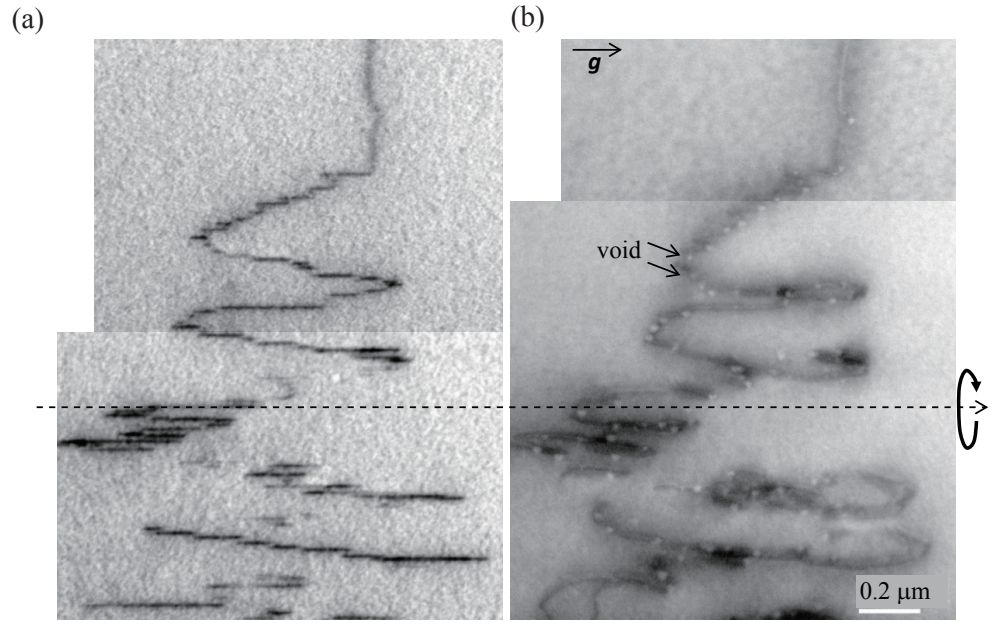

Fig. 8 BF-STEM image taken from a part of the region shown in Fig. 5, where (a) is at incidence and (b) is tilted about 20 degrees with respect to [11−20] with $\boldsymbol{g}$ = 11−20.

method. In the evaluation of in-grown vacancy defects in ammonothermal GaN synthesized via the positron annihilation method, a high concentration of Ga vacancy-related defects in n-type samples with varying free electron and oxygen content were observed.[27,28] These results support the deformation process of the helical dislocation in GaN crystals produced using the ammonothermal method. The deformation of the edge dislocation shown in Fig. 6 seems to be caused by vacancy defects, as in the case of helical dislocation.

Furthermore, in our previous work, the influence of dislocations on the leakage current of Schottky barrier diodes fabricated on an epitaxial layer was explored and it was found that the deformed dislocations and formed voids were not observed in the epitaxial layer and that the dislocations did not affect the leakage current characteristics of the epitaxial layer.[29] Thus, it is suggested that the deformation of dislocations in the GaN substrate does not adversely affect the epitaxial layer. Therefore, the low-dislocation density GaN substrate fabricated using an ammonothermal method in this study may be effective for use in high voltage devices.

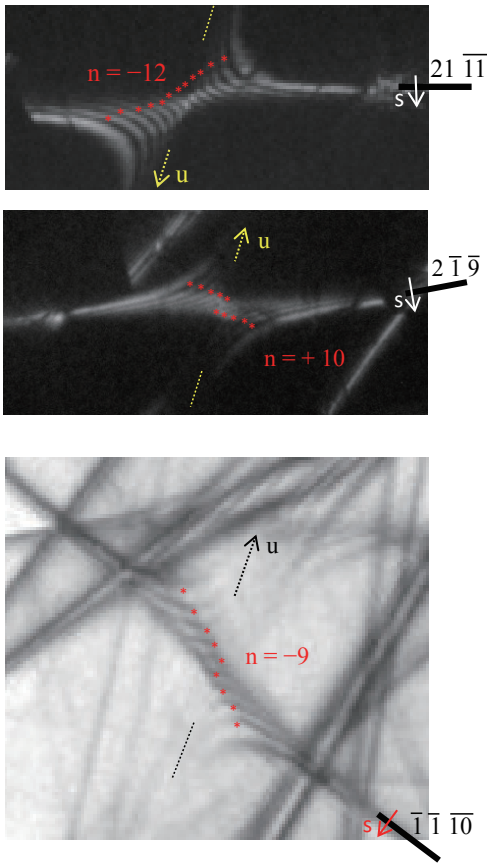

Fig. 9 LACBED images of mixed dislocations in the epitaxial layer. Dark-field LACBED image for $\boldsymbol{g}$ = (a) 21−11, (b) −2−19, and (c) Bright-field LACBED image for $\boldsymbol{g}$ = −1−1−10. The parameter $\boldsymbol{g}$ represents the diffraction vector, n represents the number of splits, s represents the excitation error, and u represents the dislocation line direction.

Table 1 The linear system of equations.

$\boldsymbol{b} = [u\ v\ w]$

	$\boldsymbol{g}_{hkl}$	$\boldsymbol{g}\cdot\boldsymbol{b} = n_{exp}$
(a)	2 1 −11	$2u + v - 11w = -12$
(b)	−2 −1 9	$-2u - v + 9w = 10$
(c)	−1 −1 −10	$-u - v - 10w = -9$

→ $\boldsymbol{b}$ = [0 −1 1]

4. Summary

Dislocation analysis was carried out on a GaN epitaxial layer on a GaN substrate fabricated using a basic ammonothermal method using synchrotron radiation XRT and TEM. Deformation “helical dislocation” and void formation by heat treatment were observed in the GaN substrate, with the helical dislocations found in a GaN crystal for the first time. These phenomena are formed by the interactions between the dislocations and vacancies. Conventional GaN crystals have a high density of dislocation; however, such crystals show no deformation. The generation of new defects was found to be driven only by heat treatment. In this study, the formation of defects similar to those found in metals, Si, and GaAs single crystals was observed, showing that the crystal quality of the GaN crystal was improved dramatically.

Acknowledgment

The synchrotron radiation experiments were performed at the BL16B2 of SPring-8 with the approval of the Japan Synchrotron Radiation Research Institute (JASRI) (Proposal No. 2011B5370, 2012A5370, 2012B5370 and 2013A5370). A part of this work was supported by Nagoya University microstructural characterization platform as a program of “Nanotechnology Platform” of the Ministry of Education, Culture, Sports, Science and Technology (MEXT), Japan.

References

(1) Lester, S. D., Ponce, F. A., Craford, M. G. and Steigerwald, D. A., *Appl. Phys. Lett.*, Vol. 66, No. 10 (1995), pp. 1249-1251.
(2) Wu, X. H., Brown, L. M., Kapolnek, D., Keller, S., DenBaars, S. P. and Speck, J. S., *J. Appl. Phys.*, Vol. 80, No. 6 (1996), pp. 3228-3237.
(3) Motoki, K., Okahisa, T., Matsumoto, N., Matsushima, M., Kimura, H., Kasai, H., Takemoto, K., Uematsu, K., Hirano, T., Nakayama, M., Nakahata, S., Ueno, M., Hara, D., Kumagai, Y., Koukitu, A. and Seki, H., *Jpn. J. Appl. Phys.*, Vol. 40 (2001), pp. L140-L143.
(4) Oshima, Y., Eri, T., Sshibata, M., Sunakawa, H., Kobayashi, K., Ichihashi, T. and Usui, A., *Jpn. J. Appl. Phys.*, Vol. 42 (2003), pp. L1-L3.
(5) Nakamura, D., Kimura, T. and Horibuchi, K., *Appl. Phys. Express*, Vol. 10, No. 4 (2017), 045504.
(6) Yamane, H., Shimada, M., Clarke, S. J. and DiSalvo, F. J., *Chem. Mater.*, Vol. 9, No. 2 (1997), pp. 413-416.
(7) Yano, M., Okamoto, M., Yap, Y. K., Yoshimura, M., Mori, Y. and Sasaki, T., *Jpn. J. Appl. Phys.*, Vol. 38 (1999), pp. L1121-L1123.
(8) Jegier, J. A., McKernan, S., Purdy, A. P. and Gladfelter, W. L., *Chem. Mater.*, Vol. 12, No. 4 (2000), pp. 1003-1010.
(9) Ketchum, D. R. and Kolis, W., *J. Cryst. Growth*, Vol. 222, No. 3 (2001), pp. 431-434.
(10) Yoshikawa, A., Ohshima, E., Fukuda, T., Tsuji, H. and Oshima, K., *J. Cryst. Growth*, Vol. 260, No. 1-2 (2004), pp. 67-72.
(11) Kanechika, M., Sugimoto, M., Soejima, N., Ueda, H., Ishiguro, O., Kodama, M., Hayashi, E., Itoh, K., Uesugi, T. and Kachi, T., *Jpn. J. Appl. Phys.*, Vol. 46, No. 21 (2007), pp. L503-L505.
(12) Kodama, M., Sugimoto, M., Hayashi, E., Soejima, N., Ishiguro, O., Kanechika, M., Itoh, K., Ueda, H., Uesugi, T. and Kachi, T., *Appl. Phys. Express*, Vol. 1, No. 2 (2008), 021104.
(13) Kachi, T. and Uesugi, T., *Sens. Mater.*, Vol. 25, No. 3 (2013), pp. 219-227.
(14) Narita, T., Ikarashi, N., Tomita, K., Kataoka, K. and Kachi, T., *J. Appl. Phys.*, Vol. 124, No. 16 (2018), 165706.
(15) Kamata, I., Nagano, M., Tsuchida, H., Chen, Y. and Dudley, M., *J. Cryst. Growth*, Vol. 311 (2009), pp. 1416-1422.
(16) Vetter, W. M. and Dudley, M., *J. Appl. Phys.*, Vol. 96, No. 1 (2004), pp. 348-353.
(17) Neudeck, P. G. and Powell, J. A., *IEEE Electron Device Lett.*, Vol. 15, No. 2 (1994), pp. 63-65.
(18) Valcheva, E., Paskova, T. and Monemar, B., J. *Cryst. Growth*, Vol. 255, No. 1-2 (2003), pp. 19-26.
(19) Pailloux, F., Colin, J., Barbot, J. F. and Grilh́, J., *Appl. Phys. Lett.*, Vol. 86, No. 13 (2005), 131908.
(20) Williams, D. B. and Carter, C. B., *Transmission Electron Microscopy: A Textbook for Materials Science* (1996), pp. 401-422, Plenum Press.
(21) Tanaka, M., Terauchi, M. and Kaneyama, T., *Convergent-beam Electron Diffraction II* (1988), pp. 160-166, JEOL.
(22) Morniroli, J. P., *Large-angle Convergent-beam Electron Diffraction* (2002), pp. 305-318, Société Française des Microscopies.
(23) Amelinkx, S. and Bontinck, W., *Acta. Metall.*, Vol. 5 (1957), pp. 345-346.
(24) Lang, A. R. and Meyrick, G., *Philos. Mag.*, Vol. 4, No. 43 (1959), pp. 878-880.
(25) Dash, W. C., *Phys Review Lett.*, Vol. 1, No. 11 (1958), pp. 400-402.
(26) Abbahams, M. S., Blanc, J. and Buiocchi, C. J., *Philos. Mag.*, Vol. 23, No. 184 (1971), pp. 795-809.
(27) Tuomisto, F., Mäki, J. M. and Zając, M., *J. Cryst. Growth*, Vol. 312, No. 18 (2010), pp. 2620-2623.
(28) Tuomisto, F., Kuittinen, T., Zając, M., Doradziński, R. and Wasik, D., *J. Cryst. Growth*, Vol. 403 (2014), pp. 114-118.
(29) Horibuchi, K., Yamaguchi, S., Kimoto, Y., Nishikawa, K. and Kachi, T., *Semicond. Sci. Technol.*, Vol. 31, No. 3 (2016), 34002.

Figs. 1-8
Reprinted from Semicond. Sci. Technol., Vol. 31, No. 3 (2016), 34002, Horibuchi, K., Yamaguchi, S., Kimoto, Y., Nishikawa, K. and Kachi, T., Formation of Helical Dislocations in Ammonothermal GaN Substrate by Heat Treatment, © 2016 IOP Publishing, with permission from IOP Publishing.

Kayo Horibuchi
Research Field:
- Materials Analysis Using Electron Microscope

Academic Degree: Dr.Eng.
Academic Societies:
- The Japan Society of Applied Physics
- The Japanese Society of Microscopy

Satoshi Yamaguchi
Research Field:
- Advanced Imaging Technique by Synchrotron Radiation

Academic Society:
- The Japanese Society for Synchrotron Radiation Research

Yasuji Kimoto
Research Field:
- Surface Analysis

Academic Society:
- The Japan Society of Applied Physics

Koichi Nishikawa
Research Field:
- Semiconductor Devices and Related Materials

Academic Degree: Dr.Eng.
Academic Societies:
- The Japan Society of Applied Physics
- Society of Automotive Engineers of Japan

Tetsu Kachi
Research Field:
- Power Electronics and Power Devices

Academic Degree: Dr.Eng.
Academic Societies:
- The Japan Society of Applied Physics
- The Institute of Electronics, Information and Communication Engineers

Award:
- JJAP Outstanding Paper Award, The Japan Society of Applied Physics, 2008

Present Affiliation: Nagoya University

